REAL-TIME VISUALISATION OF ANTENNA PATTERNS

Pau Latorre Costa

Department of Electrical and Information Technology
Lund University

Supervisor: Daniel Sjöberg

November 4, 2009

Printed in Sweden
E-huset, Lund, 2009

Abstract

In this project the real-time visualisation of antenna radiation patterns through infrared thermography is studied. This technique allows for a 2-dimensional imaging of incident power levels on the surface of a detector screen, through their temperature signature, thus revealing a region of the radiation pattern of the emitting antenna when placed at a distance.

Based on previous experiences, the design parameters of the resistive screen on which to observe the heat signature of incident microwave radiation have been studied in detail and different possible implementations have been discussed. Models of the coating for the resistive screen have been made in order to test their validity for the technique under study.

Acknowledgements

In the first place I would like to thank my tutor at LTH, Docent Daniel Sjöberg for directing my Master's Thesis and for always willing to clarify my doubts and guide me throughout these months. I must also thank the staff of the Electrical and Information Technology Department at LTH, and at the International Office, who received me in Sweden with infinite hospitality and assistance.

On the personal level I must most intensely thank my parents, Anna Maria and Jordi, excellent doctors and even better people. From them I have received love and support at all times throughout my years of education.

If I have got this far in university it is undoubtedly also thanks to my friends: it now becomes awkward to look back and think of everything we have gone through with the people at A.C. Telecogresca (I believe there is no need for names), my "other" house, the center of my life for the past five years, and the place in university where I have learnt much more than in any course.

Also, I am proud of having been a member of the family of BEST Barcelona, they showed me a totally new aspect of university, probably the one that pushed me to go abroad, and most important I became rich in the most valuable asset: friends, both in Barcelona and throughout Europe.

Last but not least, there's the people I have met in Lund some of which I knew beforehand, some of which I met in Sweden, and who have become my family during this last year.

Table of Contents

Chapter 1
Introduction

1.1 Motivation

In the field of antenna testing the general approach towards radiation pattern determination poses several disadvantages. The standard techniques require a series of repetitive and time consuming probe measurements to be made. Therefore, these techniques clearly do not allow for a real time representation of radiation diagrams and involve a complex process to be performed between two different tests.

Infrared thermography of radiation patterns is a relatively recent technique developed as an alternate system for antenna pattern determination. This method can offer, when applied to far-field testing a fast and time-efficient way to determine qualitatively the pattern of an antenna under test. The technique is based on the heating produced by incident radiation on a resistive screen the temperature of which is visualized by an IR camera. In the following chapter this technique is described in depth.

Due to its characteristics, thermographic techniques might be a feasible system to study for antenna radiation pattern representation in real time, with the possibility of its continuous monitoring. Moreover the lack of repetitive sampling and moving elements (test probe) can reduce the complexity, cost, and human resources required by standard techniques. Therefore this technique should be studied as a possibility for a simpler and more accessible system for qualitative antenna pattern determination.

1.2 Objectives and aims

This thesis has several objectives: mainly to study the feasibility and design requirements for a thermographic imaging system, including a characterisation of the ideal parameters for the device at the heart of the system, the resistive detector screen. On the basis of this design, the capacities of the system for real-time antenna pattern visualisation should be determined. Another objective in a further stage is to implement if possible the system and validate experimentally the proposed design.

To summarize, the main objectives are:

- To determine the design requirements of a thermography system for far-field visualisation of antenna patterns
- To design the system and suggest possible practical implementations
- To determine if the system is feasible for a real-time visualisation
- To implement the system and test it.

This thesis is organized as follows: In chapter 2 we present the technical background of this project, describing the test technique at its root, thermographic imaging of radiation patterns. In Chapter 3 we describe the basic setup of a thermography system, as it should be arranged for the type of visualisation we are focusing on. Chapter 4 deals with the design requirements of the most particular element of the technique, the detector screen. It is characterized electromagnetically in order to find the design values that offer an optimal behavior for the thesis' objectives.

Subsequently, Chapter 5 studies a particular possibility proposed in this thesis to modify the characteristics of the detector screen through patterns in its coating with the objective of optimization. Chapter 6 deals with the practical implementation of the system with a special focus on a tailor-made detector screen. Finally in Chapter 7 we present the conclusions of the present thesis, we propose future works, and we suggest applications and alternatives to the system under study.

Chapter 2
Background

2.1 Wireless technologies

Wireless communications are gaining importance and playing an increasingly vital role in our society. Over the last decades we have seen how communication technologies have progressively migrated from wired applications to wireless systems which make use of radio waves. Furthermore, these electromagnetic waves play an important role in many relevant fields other than the transmission of information, such as RADAR, navigation or medical diagnose among many others. We live surrounded by radio technology, and it has been one of the cornerstones of the development of society over the last century.

2.1.1 Antennas

If we talk about electromagnetic waves and radio engineering we are forced to focus on it's most characteristic and vital piece of hardware: the antenna. According to the IEEE standard definition an antenna is *that part of a transmitting or receiving system that is designed to radiate or to receive electromagnetic waves* [1]. Independently of its purpose or features, any system that makes use of electromagnetic waves must posses a radiating element, the last (or first) link in the chain of transmission (or reception).

The number of bands of the electromagnetic spectrum, each one having particular characteristics, and the many uses given to radio waves account for the wide range of architectures and implementations of wireless systems. Consequently, we are also presented with an immense range of different antenna designs, depending essentially on their purpose and working frequencies. While their shapes are very variable they all have in common that they become the region of transition between a zone where a guided wave exist, and a zone where this same wave propagates in free space[2].

2.1.2 Microwaves

Radio waves are characterized by their frequency and wavelength, both related by the speed of propagation in the medium (generally air). The set of all frequencies or spectrum is divided in bands which standardisation organisations assign to

Table 2.1: Bands of frequencies among microwaves.

BAND	FREQUENCY	WAVELENGTH
L	1 - 2 GHz	30 - 15 cm
S	2 - 4 GHz	15 - 7.5 cm
C	4 - 8 GHz	7.5 - 3.65 cm
X	8 - 12.4 GHz	3.75 - 2.42 cm
Ku	12.4 - 18 GHz	2.42 - 1.66 cm
K	18 - 26.5 GHz	1.66 - 1.11 cm
Ka	26.5 - 40 GHz	11.1 - 7.5 mm
mm	40 - 300 GHz	7.5 - 1 mm

particular applications.

Moreover, of especial relevance nowadays are microwaves, which are waves with a frequency that ranges from 300 MHz to 300 GHz. We divide microwaves in a set of bands according to the frequency range which dates back to the early days of RADAR, as seen in Table 2.1.

The present importance of microwaves resides in the fact that they are widely used in a variety of applications, such as modern GSM mobile phone networks (900 - 2100 MHz), Wireless Local Area Networks (2.4 - 5 GHz) or Global Positioning System (1.2 - 1.5 GHz), among others. In this project we focus on the lower end of the microwave spectrum, thus when citing our frequencies under study we are referring to the 1 - 10 GHz band. We concentrate our study in this particular range because within it we find functioning many of the most flourishing wireless applications orientated towards the general consumer market.

2.2 Antenna characterisation

Antennas can be characterized taking into account different parameters. In general, the application for which an antenna is purposed imposes certain requisites on the region of space onto which energy is radiated. On the same way, antennas have to be capable of detecting waves from a certain region and absorb their energy efficiently in order to hand them onto the receiver.

From a broad perspective we can group the antennas within the following types[2]:

- **Wire antennas:** Made of conducting wires than generate radiated fields.
- **Aperture antennas and reflectors:** The generation of the wave is achieved through a field distribution on the antenna and are usually excited with wave guides.

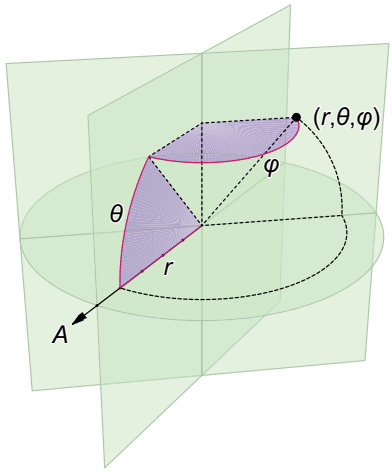

Figure 2.1: Representation of the variables in a spherical coordinate system, the most widely used for radiation pattern expression.

- **Antenna arrays:** The combination of several radiating element to achieve custom radiation patterns which are impossible to produce with one single element.

We can in a general sense define two missions for an antenna: to transmit and to receive. Moreover, we can go deeply into their features and study their different parameters, such as the power levels they must tolerate, their radiation pattern, their polarization, the operating frequency or their radiation and ohmic resistances.

Out of the set of parameters of an antenna, one of the most relevant for the present project is the radiation pattern or diagram. It is described as the representation of the radiation properties of the antenna in function of the different directions in space. Therefore, radiation patterns can be used to visualize which regions of space receive higher power densities and which receive lower as seen from the antenna. Due to the reciprocity theorem antenna patterns also apply for reception, describing in which directions antennas absorb more efficiently radiation, thus allowing for directional discrimination.

Radiation patterns are generally expressed in spherical coordinates with the origin on the antenna, and constant distance (Figure 2.1). Therefore, electric field or power is expressed in relation to the angular variables. It is common however, that their graphical representations are expressed as 2D cuts, such as the example in Figure 2.2.

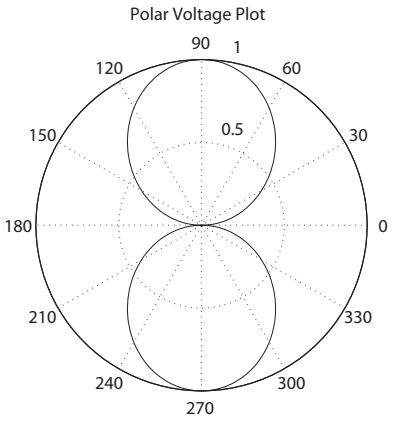

Figure 2.2: 2D cut of an spherical radiation diagram for a 1/2 wavelength wire.

2.3 Antenna pattern testing

Taking into account the nature and objectives of this project, we now study the traditional approach towards antenna testing. Among the different parameters of an antenna, the most commonly tested for, and the one which requires a higher degree of technical complexity is the radiation pattern. In fact, antenna testing has developed into its own field within radio engineering, as a speciality and a business onto which research institutions and companies concentrate their activity.

The general method for the determination of radiation patterns involves moving a second antenna, named probe, around the antenna under test. The distance between the two is kept constant while the received signal at different angular positions is recorded, as seen in Figure 2.3. In practice, this method is usually implemented by fixing the probe and rotating the antenna under test around the two angular variables.

It is common in applications where intensive antenna testing is conducted that the actual rotating movement of the antenna under study is steered by computer controlled electromechanical systems rather than relying on human operators. These systems allow for the radiation pattern testing to be a mainly automatic process.

The described method however, poses a number of disadvantages. One of the most relevant is the fact that this technique records just a discrete number of samples. Therefore, it doesn't obtain a true full representation of the radiation pattern but a series of values at certain angular directions from where the pattern is estimated. It is provable however, that the function representing the radiation diagram of an antenna is of limited spectrum. The bandwidth of this spectrum is a function of the electrical size of the antenna. Therefore with a correctly chosen sampling rate (angle increment) it is possible to reconstruct the diagram for any

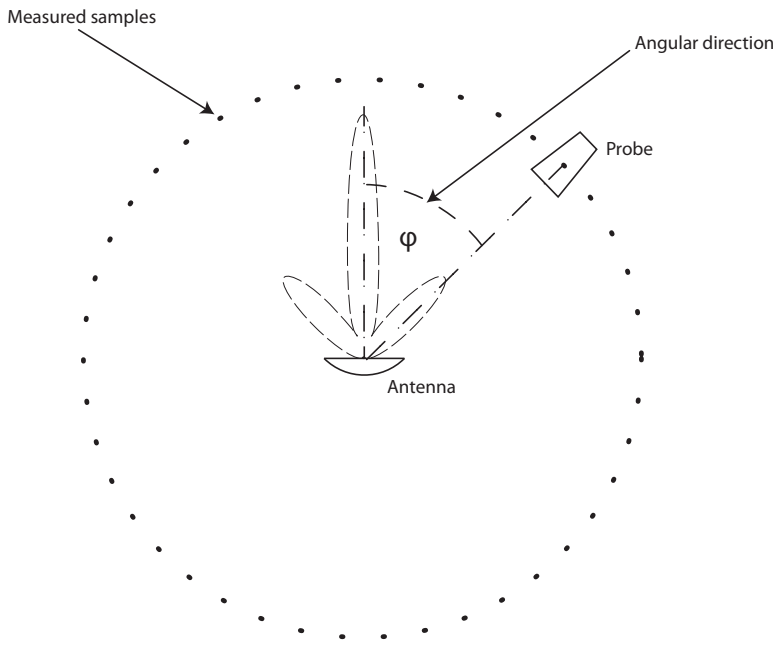

Figure 2.3: Depiction of radiation pattern sampling with a moving probe around the antenna under test at constant radius.

direction in space by using interpolation techniques [2].

Another notable disadvantage of the usual method is the fact that it is extremely time consuming and representations cannot be obtained on real-time. This is explained by the fact that a complete determination of a pattern requires a full set of samples to be taken, thus the full process of characterizing the radiated field at certain angular positions has to be repeated for any modification done on the antenna.

2.3.1 Testing range

When referring to antenna testing one of the most important issues to focus on is the testing range. With the objective of achieving precise radiation pattern determination, deep attention has to be payed to the elimination of interference which modifies the results of the measurements. This interference can involve radiation from external sources invading the test range, or unwanted reflections from the antenna under study or testing equipment.

Even though a series of configurations of free space test ranges are defined on the IEEE Standards on Antenna Testing [3], the one type of range that provides better control on testing conditions and interference reduction is the anechoic chamber. These are closed rooms where the walls and any source of reflection (such

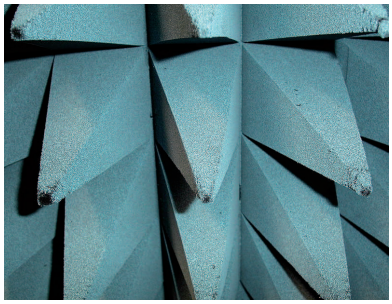

Figure 2.4: Pyramids of RAM on the walls of an anechoic chamber. *Author: Bryan Tong Minh, distributed under the GNU Free Documentation License.*

as test equipment) are fully covered by Radiation Absorbent Material (RAM) with the objective of dissipating the power of incident waves in order to minimize the reflections which might interfere with the measurements. In general these RAM are made up of a lossy material forming periodic pyramids as depicted in Figure 2.4. The optimal size of these pyramids is in the order of the wavelength under study. RAM materials play an important role in the present project, and we therefore elaborate deeper on them in the following section.

Auxiliary structures (such as supporting pedestals) are usually also covered with RAM coating and made of low-reflecting materials such as wood. Moreover, in order to protect from interference of external sources, the whole structure of the anechoic chamber is usually shielded by a Faraday cage.

2.4 Thermographic imaging

Alternate methods have been developed that can be of use for antenna pattern determination. In this project we study the implementation of thermographic imaging for real-time visualisation of antenna patterns. This method was initially developed in the 1980's within the work by Professor R.M. Sega, and eventually continued by Professor J.D. Norgard both from the University of Colorado (USA) [5].

Thermographic imaging offers a non-invasive system for mapping electromagnetic fields. It does so by employing a low-conductivity surface on which radiation from the antenna under test penetrates. Incident electric fields generate currents on the surface which at the same time produce heat through the well known Joule Effect.

The mechanics behind pattern determination are simple: points of the surface that absorb higher levels of electromagnetic radiation show higher temperature increase, thus the representation of temperatures on the surface reveals the dif-

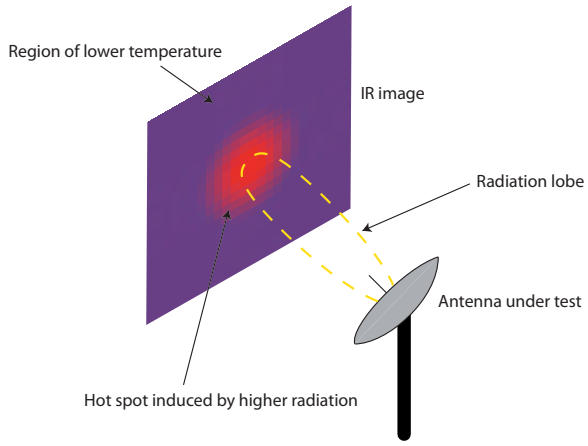

Figure 2.5: Mock up of an IR visualisation representing hotter areas on the conductive screen where incident power is higher.

ferences between incident radiation levels. This temperature pattern is therefore revealing the antenna radiation pattern. The method used to visualize this pattern is an IR camera which represents false color images of temperature differences. A mock-up of this visualisation method can be seen on Figure 2.5.

Often, this technique has been used for near-field determination, which through iterative algorithms (where several distanced planes are imaged) achieve phase retrieval [5, 7, 10]. With these algorithms far-field patterns are determined from near-field characterisation. In this project however, we study the more simple far field IR visualisation, even though this technique poses the challenge of the lower power reaching the Fraunhofer region.

Comparisons can be established between the standard testing method and thermographic imaging. This system makes no use of a probe which acts as an antenna. In fact, the probe antenna becomes the low-conductivity detector screen by absorbing incoming electromagnetic waves. The different temperatures on the screen can be seen as a 2-dimensional set of punctual power levels from the standard probe.

We can notice one of the main advantages of this system: while in the standard method we need a number of samples to be taken to characterize a region of the radiation pattern, with the thermographic method one only IR image can reveal a portion of this pattern only limited by the size of the detector screen. As the detector surface has an infinite number of points, we could argue that each image is taking an infinite number of samples of incident power. In practice this is limited by the resolution of the IR camera and the heat conduction in the screen.

It is clear that this process cuts dramatically the time employed in each measurement. In fact, if there is a low delay between a variation of the incident field

and its translation into temperature differences this system could be employed for continuous monitoring in real-time of a radiation pattern. As an example, this system should be able to follow a moving antenna as its lobes move over the surface of the detector screen. In this project we study possible implementations of the system and their viability.

2.4.1 Radiation absorbent materials

We have previously commented on radiation absorbent materials, such as the pyramids which coat the walls in anechoic chambers. Moreover, this kind of materials are also in the base of thermographic imaging. In general radiation absorbent materials are intended to absorb incoming electromagnetic radiation with the objective of minimizing transmitted and reflected waves. We can see an example of this use in RADAR stealth technologies where these materials coat sensitive parts of vehicles in order to hide them from RADAR detection.

The fact that this materials dissipate the energy they absorb from electromagnetic radiation in the form of heat through Joule Effect is usually regarded as an undesired by-product of wave attenuation [4, p. 298]. In this project however we study the properties of these materials to absorb waves in the form of heat as a desirable phenomenon and its final objective. We therefore study the possibilities to implement and design a radiation absorbent material which suits the needs of the thermographic method for real time visualisation of incident electromagnetic fields.

Chapter 3
Basic setup

We initially discuss a possible implementation of the basic setup of the system under study, the function of which is to determine the radiation diagram for an antenna under study. We do this, as previously commented, by observing the heat signature produced by incident microwave radiation on a detector surface in real time. The frequency range which we focus on in this project is 1 - 10 GHz.

3.1 Detector screen

The central role in the system under design is played by the surface on which the microwave radiation from the antenna under test incides. This surface absorbs a part of the radiated energy, developing temperature differences that can be visualised in real time by an IR detecting camera. Sections of the sheet where incident power density is higher should show a higher temperature difference. On the other hand sections where microwaves incide with less amplitude should show less (or even no) increment on temperature thus revealing the radiation diagram. This is achieved by employing a surface coated with a material of a certain thickness and conductivity. These properties are studied further in depth in Chapter 4.

A structure is proposed with a squared or rectangular-shaped, flat, rigid surface, made of a material which is transparent to microwaves, such as poster board. This surface holds a sheet of paper or film coated with the material that acts as a detector of the microwaves, as shown in Figure 3.1. A variation of this implementation would be to coat directly the rigid surface with the detector material.

3.2 Elements arrangement

The arrangement of the different elements involved in this system is based on previous experiences [5, 6, 7, 8, 9, 10, 11, 12, 13]. As in usual radiation pattern characterisation the testing procedures should take place in an anechoic chamber as a means of preventing reflections from walls which can return to the screen and increase the apparent power inciding on its surface. Also the shielding of the chamber prevents external interference which can compromise the validity of the

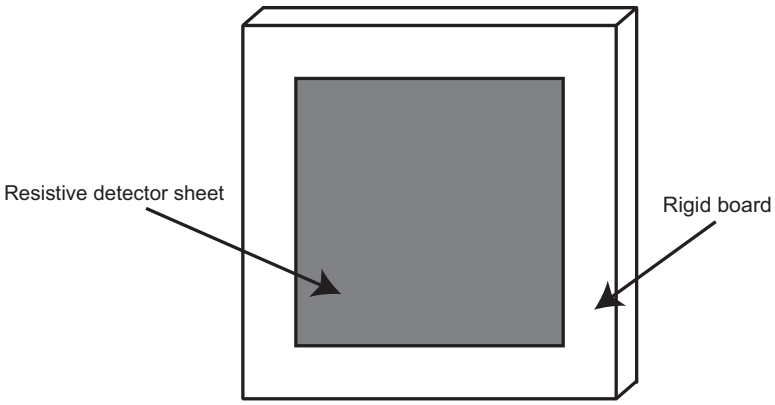

Figure 3.1: Detector sheet on rigid board.

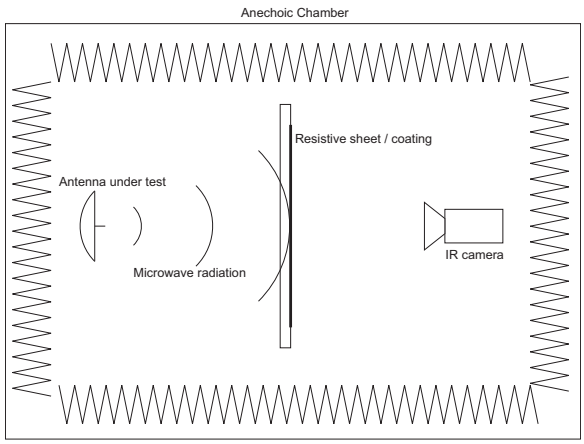

Figure 3.2: Overhead diagram of the basic arrangement of elements.

measurements.

The antenna under test should be placed with the region of interest of its radiation pattern facing one of the two flat sides of the detector screen. For the IR camera not to disturb the measures, the flat side holding resistive sheet is proposed to be facing the opposite side of the antenna. Due to the transparency to microwaves of the holding board, the orientation of this sheet would not affect the results. At an edge of the setup the camera would face resistive sheet as depicted on the overhead view diagram in Figure 3.2.

One factor to consider is the unwanted effect of reflections from the camera if it contains sensitive parts where backscattering can happen. In this sense it could be set slightly displaced from the axis, and oriented at an angle in order to avoid backscattering towards the resistive sheet and the antenna as seen in Figure 3.3. This would deviate possible incident waves backscattered from the camera onto

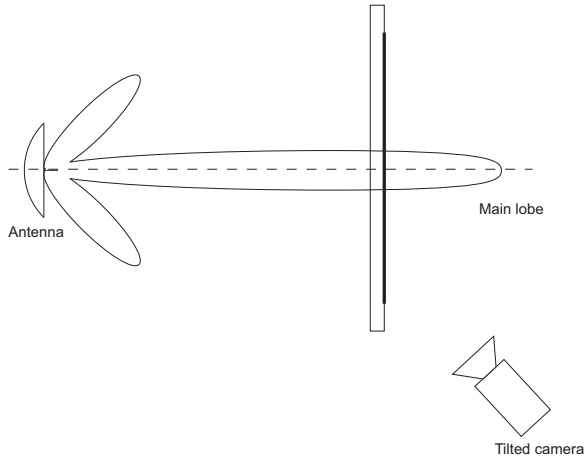

Figure 3.3: By displacing the camera and facing it at an angle towards the detector sheet we can prevent unwanted backscattered reflections that affect the test.

the chamber's absorbing walls. Also displacement of the camera could help avoid main lobes thus minimizing incident power into it. While the thermographical image would be taken at an angle the plane representation could be achieved by simple image processing techniques.

This suggested setup, would have as a main drawback the fact that a plain sheet at a distance from the test antenna would only be able to show an IR visualisation of the illuminated portion of the radiation pattern. While in general cases, the test would be performed to observe only regions of interest within the pattern (usually main lobes), a full characterisation would imply testing all directions where radiated power is not null. To achieve this level of characterisation the detector sheet could be rotated around the antenna through manual or mechanical means, as depicted in Figure 3.4, thus covering every direction of interest within the solid sphere surrounding the test device.

3.2.1 Antenna-Screen distance

Regarding the distance at which the detector screen should be situated from the antenna, we must take into account that we wish to detect the radiation pattern. Therefore, we place the screen, and thus observe the radiation signature on the Fraunhofer region. Consequently it should be placed at a distance higher than Fraunhofer's

$$d = \frac{2D^2}{\lambda} \tag{3.1}$$

where D is the biggest dimension of the antenna and λ is the wavelength.

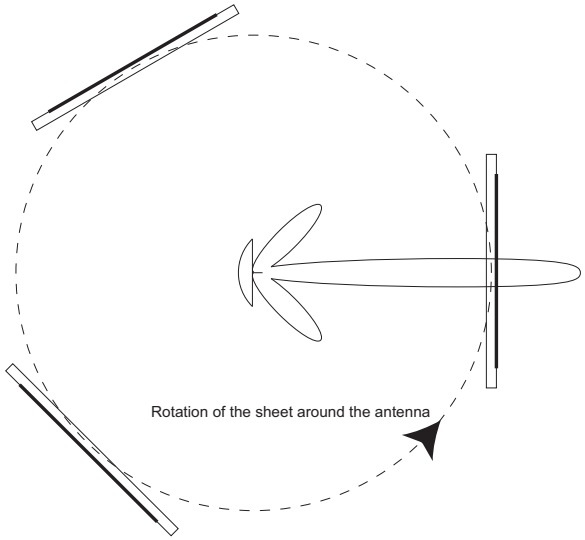

Figure 3.4: Characterisation of the complete radiation pattern with a limited size flat detector sheet can be achieved by rotating it around the antenna under test.

Chapter 4

Detector sheet design

4.1 Detector sheet design

The main challenge of the current project is to achieve a satisfactory design of the detector screen. Initially, we discuss the required properties of the sheet's coating for the system to perform as intended. The first factor to take into account is the minimization of radiated energy which is backscattered from the screen. Eventually, we also study how energy is absorbed and transmitted, and how this absorption has an effect on the temperature of the screen.

Previous experiences with thermographic imaging have usually relied on existing commercial coated papers, the characteristics of which (specially conductivity) suit the objectives of the setup. We study these characteristics and discuss possible tailor-made implementations of the conductive coatings.

4.2 Conductive coating

The root of the antenna characterisation method under study is the conductive properties of the coating on the detector screen. It is based on the fact that incident electromagnetic fields on a surface induce current densities depending directly on the material's conductivity and the intensity of the field. These currents at the same time produce an increase in the temperature on the material which we can record through direct measurement or, as in this method, through infrared thermography.

As we study in detail further into this chapter the two main variables that affect how incident microwave radiation backscatters and builds temperature on the screen are conductivity and thickness. We can consider that thickness depends basically on the coating method, therefore different techniques provide different possibilities regarding the coating depth. The controllability of the thickness therefore is determined by the coating method employed, but it is arguable that we might only have available a discrete range of thicknesses. It is also an issue to take into account that even though a uniform thickness coating might be achieved, difficulties might arise to determine its value [5]. On the other hand conductivity

is linked directly to the coating material used.

In previous experiences from various authors such as [5, 9, 10] the chosen materials for the detector screen have been carbon or graphite papers or polyamide. The conductivity of the coatings on the paper together with their thickness have proved to be suitable for the observation of microwave incidence through thermography. Some of these papers are available commercially through education supplies providers, such as Teledeltos papers. This type of paper is widely used in schools and college laboratories as their coating can map currents through color change on their surface when voltage differences are applied. The resistive element on this sheet is a thin layer of coated graphite powder.

The conduction properties of graphite powder make it one of the most suitable coatings for the system under study. It is commonly used in applications or experiments where a surface must be covered with a resistive coating such as [14], used as the main ingredient of a resistive paint. In Norgard's experiments [8, 9, 10], for example, the graphite coated paper had a conductivity of 8 S/m. As we later discuss the values achieved with graphite coatings are within the range for the desired specifications on this project.

Due to lack of availability of suitable graphite coated papers, as discussed in 6, we study the possibility of creating through a simple procedure our own coating based on commercially available paint and graphite powder.

4.3 Backscattering

As previously stated, one of the first design requirements to study regarding the resistive screen is the avoidance of backscattering towards the source antenna under test. Taking into account the fact that a main objective is for as much radiated power as possible to be absorbed and converted into heat on the sheet, we expect to minimize the losses through reflection. We, on a second stage, discuss what fraction of the power which is not backscattered is actually absorbed and converted into a temperature increase.

Furthermore, as described on the IEEE Standard Antenna Test Procedures [3], reflection from the test antennas (in our case the resistive sheet) is a possible source of error for the determination of the received amplitude levels, specially, those of the main lobe. It may therefore modify the recorded antenna pattern, a clearly undesired effect.

4.3.1 Circuit analogue

For the previously stated reasons, the initial concern in the development of this project is to study ways of determining how incident waves are backscattered from the sheet and eventually minimize the effect. With this objective a circuit analogue is used as suggested in [15] in order to provide simple means to study the reflection towards the source in the experimental set-up. This equivalent model

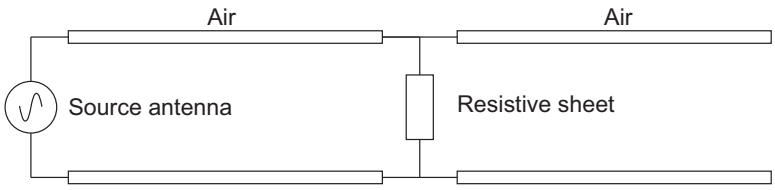

Figure 4.1: Analogue circuit model

treats the transmission medium (air) as a transmission line with characteristic impedance Z_0 and the antenna as a wave source.

The value left to be determined is the resistance to assign to the inserted element equivalent to the presence of the resistive sheet. In this case we can refer again to [15], and treat a thin sheet as an impedance with a certain sheet resistance

$$R_S = \frac{1}{\sigma d} \tag{4.1}$$

where σ is the conductivity of the material and d is its thickness. If as expected a sheet of squared proportions is implemented, we can assign the sheet resistance as the element's impedance. Therefore the analogue circuit model of the setup would be as shown in Figure 4.1.

This analogue, where the inserted resistive sheet is treated as a resistance is valid only if its thickness dimension can be considered electrically small. In our proposed test case, for the 1 - 10 GHz the restriction we impose is that the shortest wavelength inside the resistive material should be considerably longer than the thickness of the sheet. As we study more in depth further into the project this condition poses no problems if the correct set-up parameters are carefully chosen.

4.3.2 Load impedance

Through this model we can characterize the behavior of the incident waves on the lumped element (resistive sheet). More precisely we are interested in determining the reflection coefficient towards the load. For the computation of this parameter the equivalent model is approximated with the load being an impedance result of the parallel between the lumped element and the characteristic impedance of the empty space behind the sheet (which behaves as a matched transmission line), as seen in Figure 4.1.

We therefore need to determine the characteristic impedance of the transmission line in our model, which matches the propagation of waves through empty space/air towards the resistive sheet. Consequently, the characteristic impedance of the transmission line is that of empty space (also approximately that of dry air) $Z_0 = 120\pi\Omega$.

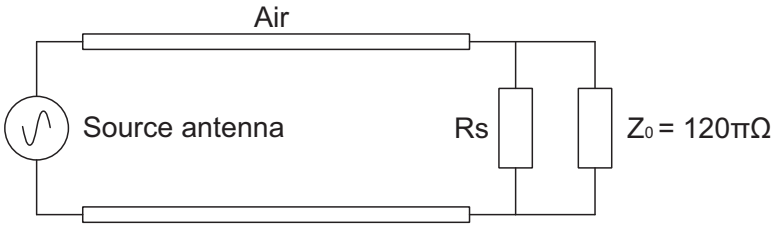

Figure 4.2: Equivalent impedance at the load

4.3.3 Reflection coefficient

The obtained equivalent model allows us to characterize the behavior of the incident waves, through the application of the reflection coefficient on the load as seen from the transmission line.

$$\Gamma = \frac{Z_L - Z_0}{Z_L + Z_0} \tag{4.2}$$

$$Z_L = R_S || Z_0 = \frac{R_S Z_0}{R_S + Z_0} = \frac{\frac{Z_0}{\sigma d}}{\frac{1}{\sigma d} + Z_0} = \frac{Z_0}{1 + Z_0 \sigma d} \tag{4.3}$$

We can therefore express the reflection coefficient as a function of Z_0 and the σd product.

$$\Gamma = \frac{\frac{Z_0}{1+Z_0\sigma d} - Z_0}{\frac{Z_0}{1+Z_0\sigma d} + Z_0} = \frac{\frac{1}{1+Z_0\sigma d} - 1}{\frac{1}{1+Z_0\sigma d} + 1} = \frac{\frac{-Z_0\sigma d}{1+Z_0\sigma d}}{\frac{2+Z_0\sigma d}{1+Z_0\sigma d}} \tag{4.4}$$

$$\Gamma = \frac{-Z_0 \sigma d}{2 + Z_0 \sigma d} \tag{4.5}$$

This formula provides the means to determine the amount of incident radiation that is backscattered. From it we can clearly see that in the test conditions the parameter which is tunable, and therefore allows us to optimize the reflection is the resistance of the sheet, dependant at the same time on the σd product.

We can consequently plot the reflection coefficient as a function of σ and d, using the value of Z_0 of air, as seen in Figure 4.3. Besides, and taking into account the relation between sheet resistance, thickness and conductivity previously stated, we can show graphically the dependance of reflection coefficient with R_S (Figure 4.4).

Out of all the power density that reaches the resistive screen, we can now express that a fraction $|\Gamma|^2$ is backscattered, and a $1-|\Gamma|^2$ fraction is actually transmitted. We must also study, however, which fraction of this remaining power is absorbed and therefore may be transformed into heat on the resistive material. This is discussed on the following section.

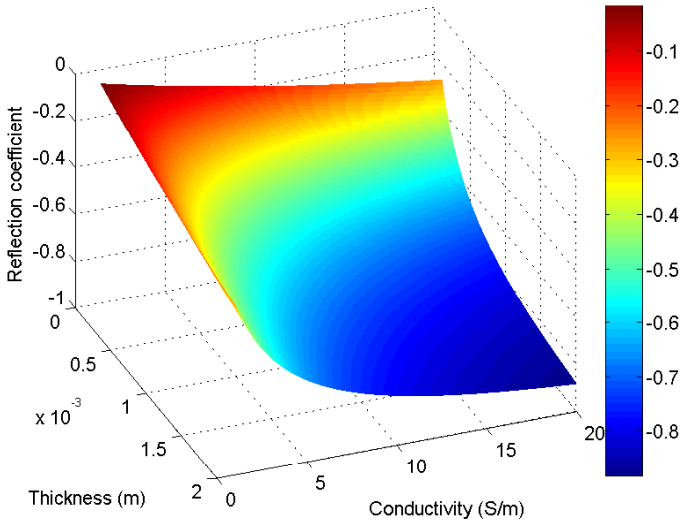

Figure 4.3: Surface plot of the dependance of reflection coefficient to conductivity and thickness.

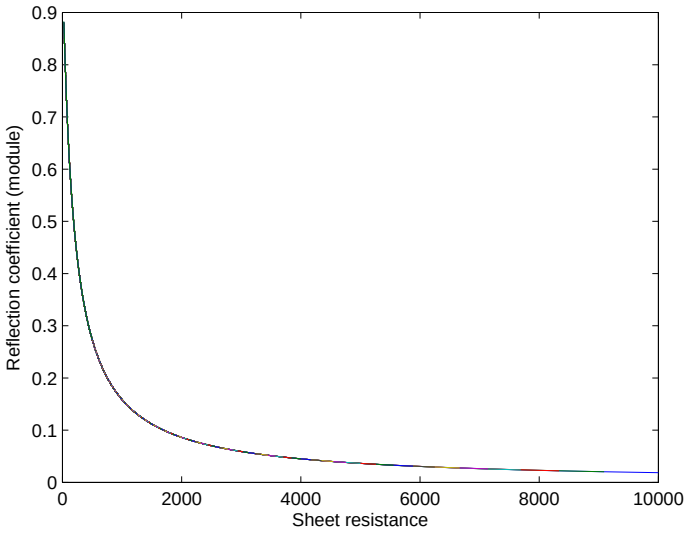

Figure 4.4: Dependance of the module of reflection coefficient to sheet resistance.

4.4 Power absorption

So far we have dealt with the characterisation of backscattering from the detector screen in order to minimize the loss of power through reflection. Once again, it is worth taking into account that our final objective is to absorb as much radiated power as possible on the conductive coating. This absorbed power heats the surface of the screen and therefore we are able to detect the heat trace of the microwave radiation.

In this section we study, out of the incident power which is not reflected, which fraction is actually absorbed, and therefore plays a role in the heating of the detector surface, and which fraction is transmitted through it, and therefore dissipated into open air (or the chamber's absorbing walls).

As discussed widely in previous experiences[9], the general expression for absorbed power inside the lossy material (resistive sheet) is

$$P_{abs} = \frac{1}{2}\int_V (\sigma|E_{tot}|^2 + \omega\varepsilon''|E_{tot}|^2 + \omega\mu''|H_{tot}|^2)\mathrm{d}V \tag{4.6}$$

where E_{tot} and H_{tot} are the electric and magnetic components of the electromagnetic field taking into account the effects of reflection,

$$E_{tot} = E_{inc}(1+\Gamma) \tag{4.7}$$

ε'' and μ'' are the imaginary components of permittivity and permeability of the material, σ is the conductivity of the material, and ω is the angular frequency of the incident electromagnetic field.

In the frequency range we are working on, we can neglect the effect of the imaginary components of permeability and permittivity as the main determining factor for power absorption is electric conductivity[9]. We are therefore left with the following expression for power absorption

$$P_{abs} = \frac{1}{2}\int_V (\sigma|E_{tot}|^2)\mathrm{d}V \tag{4.8}$$

Through the implementation of the transmission line approximation we have been studying so far (where the thickness of the sheet waves have to go through is very small in relation to the wavelength), the module of the electric field can be approximated as constant. This leaves us with the following expression, where d is the thickness and A is the area of the sheet,

$$P_{abs} = \frac{|E_{tot}|^2\sigma dA}{2} \quad \left[\frac{W}{m^2}\right] \tag{4.9}$$

This result is coherent with the transmission line model, where the power absorbed at the load (resistive screen) can be expressed as the square of the wave amplitude (in the model, electric field amplitude is equivalent to voltage amplitude as shown in Figure 4.5) divided by the load impedance.

$$P_{abs} = \frac{|V|^2}{2R_S} = \frac{|V|^2\sigma d}{2} \Longrightarrow P_{abs} = \frac{|E_{tot}|^2\sigma dA}{2} = \frac{|E_{tot}|^2 A}{2R_S} \tag{4.10}$$

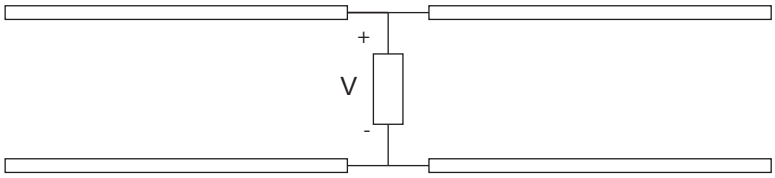

Figure 4.5: We can establish an equivalence between the voltage difference at the load and the electric field amplitude at the resistive screen for power absorption computation.

4.5 Absorption coefficient

So far, we have calculated the fraction of power incident on the resistive screen that is lost from backscattering. We have also expressed how power is absorbed on the resistive sheet. Therefore, by combining both expressions, we are able to calculate what amount of the total incident power is absorbed, and therefore can build heat.

As we have studied, the electric field on the resistive coating is made up of an incident and a reflected field

$$E_{tot} = E_{inc}(1 + \Gamma) \tag{4.11}$$

and in the particular conditions we have studied, Γ is always negative, therefore representing the fraction of reduction of the electric field module. Based on the calculated dependance of Γ on σd we can calculate

$$1 + \Gamma = \frac{2 + Z_0\sigma d}{2 + Z_0\sigma d} + \frac{-Z_0\sigma d}{2 + Z_0\sigma d} = \frac{2}{2 + Z_0\sigma d} \tag{4.12}$$

This expression indicates the fraction of electric field amplitude remaining due to backscattering losses. We want, however, to determine the remaining radiation in the form of power (surface density), so the expression must be raised to the square

$$|1 + \Gamma|^2 = |\frac{2}{2 + Z_0\sigma d}|^2 \tag{4.13}$$

which we can graphically represent in Figure 4.6.

By combining both achieved expressions, the first one describing the remaining power from reflection, and the second describing absorption, we can calculate which fraction of the total incident power is absorbed by the screen under study. We can then express a total absorption coefficient

$$\alpha = \frac{P_{abs}}{P_{inc}} = (\frac{2}{2 + Z_0\sigma d})^2 \frac{Z_0\sigma d}{2} \tag{4.14}$$

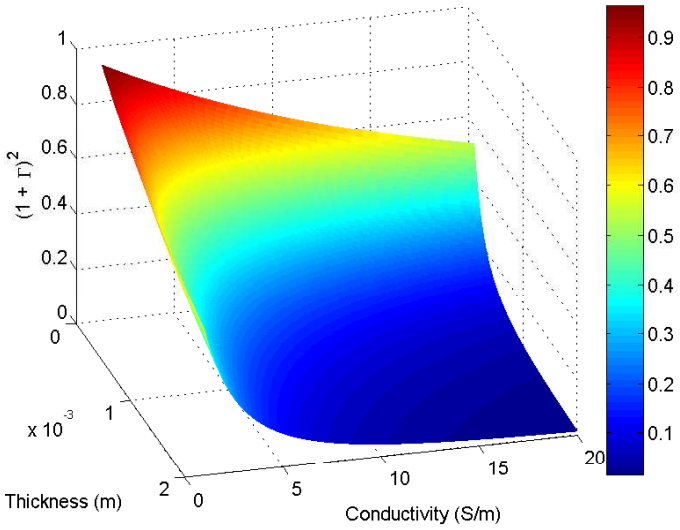

Figure 4.6: Surface representation of the contribution of reflection to total power on the screen in the form of $|1 + \Gamma|^2$.

This α coefficient is represented in Figure 4.7, as function of σ and d. It clearly shows a peak of maximum absorption which is 25% of total incident power. This region of maximum absorption is situated around the region where the σd product has a value of 0.0053 S, as seen in Figure 4.8. This value is equivalent to achieving a sheet resistance of $Z_0/2$, as expressed in Section 4.3.

4.6 Analogue validity band

So far we have based our development on the premise that we can approximate the equivalent resistance of the sheet on the load to $\frac{1}{\sigma d}$. As previously stated, this approximation is only valid as long as the thickness of the sheet is electrically small in relation to the wavelength. We therefore should determine on which margin of frequencies we can use this approximation. As seen in Figure 4.2, for a resistive sheet on a reflection-less test range, surrounded by air, the impedance at the load is equivalent to the parallel of the sheet's resistance R_S, and the characteristic impedance of the line behind the screen (in general free space), Z_0.

We can, using the formula for the single slab as seen in [16, p. 160-161],

$$Z = \eta_1 \frac{\eta_0 + j\eta_1 tank_1 l_1}{\eta_1 + j\eta_0 tank_1 l_1} \tag{4.15}$$

determine the input impedance in function of the frequency. According to our approximation, there is a low band where the input impedance is approximately that of the thin sheet approximation ($R_S//Z_0$), and as frequency increases, and

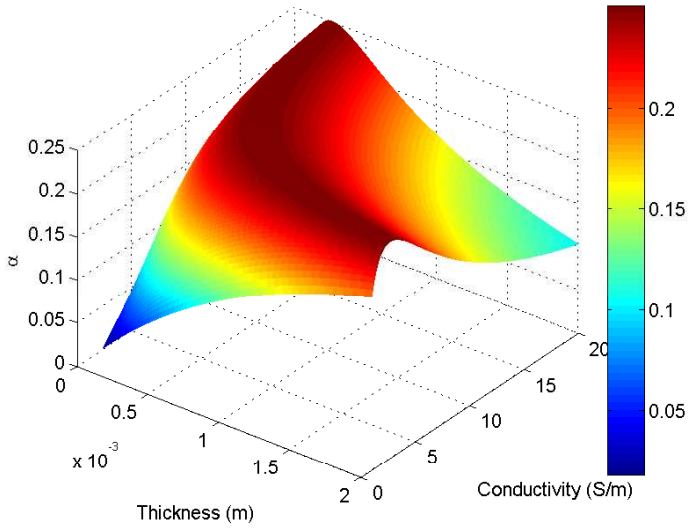

Figure 4.7: Surface representation of absorption coefficient α. Notice the peak of maximum absorption.

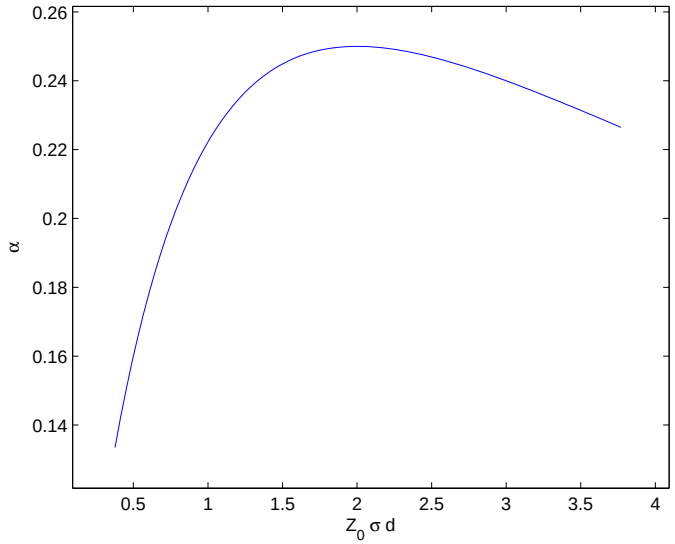

Figure 4.8: Plot of the dependance of alpha to the $Z_0\sigma d$ product, where the maximum absorption region is visible around $Z_0\sigma d \simeq 2$.

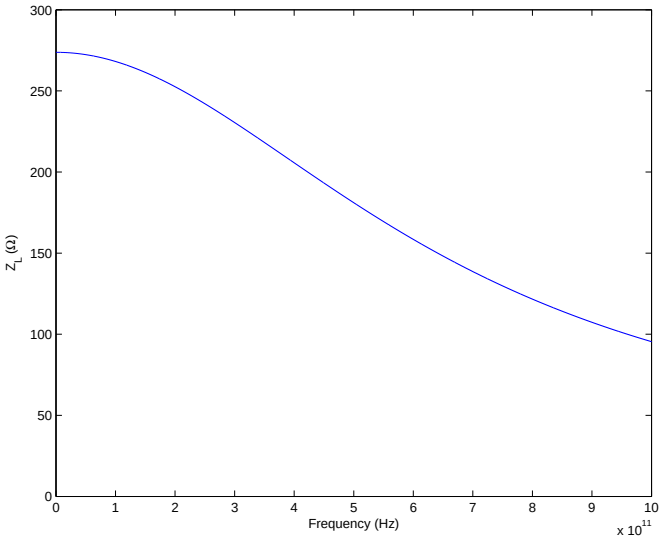

Figure 4.9: Frequency dependance of the impedance towards the resistive sheet with values d = 100 μm and σ = 10 S/m. We can see that on our band of interest the sheet resistance approximation can be considered valid.

therefore wavelength stops being comparatively bigger than thickness, both values diverge.

We can plot the frequency dependance of the load impedance of a sheet 100 μm thick and with a conductivity of 10 S/m, both values in the order of those employed in available literature. This plot is shown in Figure 4.9 and proves that for the low band approximately under 100 GHz the Z_L is approximately 273 Ω which is coherent with the approximation $\frac{1}{\sigma d}//Z_0 \simeq 273\Omega$. As in this project we are focusing on the 1 - 10 GHz band, there is a wide safe margin to use the circuit analogue with the equivalent resistance.

4.7 Screen temperature increase

In the previous sections of this chapter we have been studying how power is absorbed by the resistive screen in the set-up. The final objective of this study is to determine if and how the absorption of incident microwave radiation produces an increase of temperature on the screen's surface. If this increase is relevant in terms of detectability, it will prove that the differences in temperature on the resistive coating can reveal the radiation pattern of the emitting antenna thus allowing for its real time visualisation. Therefore, we now study the effect of incident radiation on the temperature increase of the screen.

The relation between power absorption and temperature increase on a thermographic imaging set-up has been widely studied. Several approaches have been suggested. Of particular interest due to it's simplicity is Norgard's approach [8], which has been consequently applied by other several authors [6, 7]. In this project we are taking into account this approach.

As previously described the resistive screen is absorbing power according to the expression

$$P_{abs} = P_{inc}\alpha = P_{inc}(\frac{2}{2 + Z_0\sigma d})^2 \frac{Z_0\sigma d}{2} \tag{4.16}$$

This absorbed power produces, due to the Joule effect a transient temperature build up on the surface of the screen. The increase however is halted at a certain temperature and a final stable value is reached. This happens when the achieved temperature is such that all absorbed power is lost through processes other than heat build up. These particular processes are the three possible forms of energy loss in our set-up: convection, conduction and radiation.

Convection can be described as the loss of heat through the materials surrounding the screen. In our case, for our suggested particular set-up, convection happens onto the air in contact with the coating's surface, and the rigid supporting board. The particular expression for losses through convection is

$$q = hA(T_s - T_a) \tag{4.17}$$

where q is power in W, A is surface area, T_s is screen temperature and T_a is environment temperature. The number h is the convective heat transfer coefficient in W/(m^2·K), which depends on the particular set-up of the test. Norgard uses a value of h = 0.93 W/(m^2·K) determined experimentally, for a set-up with high similarity to the one we propose. As the objective of this study is to determine viability and focus on orders of magnitude more than precision we can approximate this value as h = 1.

As mentioned, a second process through which energy is lost is radiation. As seen in [10], radiated power can be expressed in a first order approximation due to the difficulty of a precise computation for a test set-up such as the one under study. Therefore we can approximate radiated energy as

$$q = \varepsilon_{ir} A \sigma_b (T_s^4 - T_a^4) \tag{4.18}$$

where ε_{ir} is the emissivity of the radiating body, which depends on the materials properties. For carbon black coatings it is in the proximity of 0.88[17]. We can approximate this as 0.9, as for non-black bodies (real conditions) $\varepsilon_{ir} < 1$. σ_b is the Stefan-Boltzmann constant (5.669E-8 W/m^2·K^4).

One last source of thermal losses is conduction of heat, from warmer to cooler regions, in the material under study (screen). This effect can distort the visualisation of hot (more incident power) regions, diminishing the contrast between

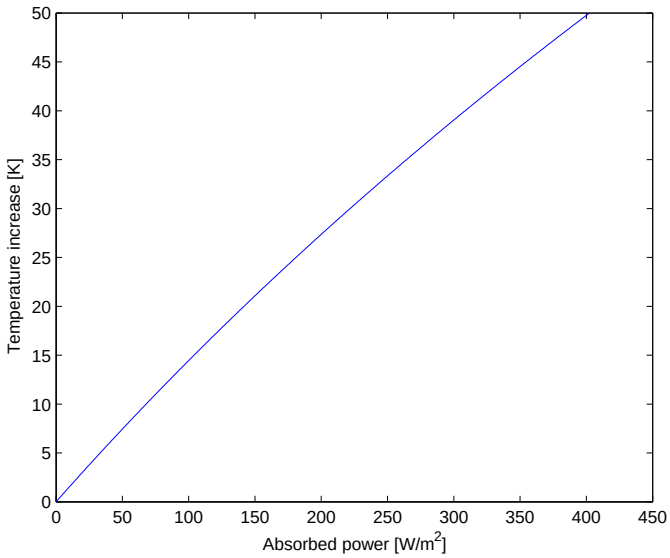

Figure 4.10: Relation between incident power density and temperature increase.

these and colder regions, creating a colour blurring effect. Conduction depends entirely on the material's properties. Previous works [9] have stated that for low-conductivity materials such as the ones involved in this project thermal conductivity is also low, and in this conditions the effect of losses through conduction can be considered negligible.

4.7.1 Thermal equilibrium

We have stated that the increase in screen temperature at one particular point on the surface is halted and a stabilisation of the heat build is reached when an equilibrium is achieved between absorbed power, and losses through radiation and convection

$$\frac{P_{loss}}{A} = h(T_s - T_a) + \varepsilon_{ir}\sigma_b(T_s^4 - T_a^4) \tag{4.19}$$

where this is expressed as a surface density at any particular point. Therefore this equilibrium is reached when

$$\frac{P_{loss}}{A} = \frac{P_{abs}}{A} = h(T_s - T_a) + \varepsilon_{ir}\sigma_b(T_s^4 - T_a^4) \tag{4.20}$$

As a matter of simplification we can assume the value of environment (room) temperature T_a to be 300 K. We are, with this expression (approximation), able to represent the relation between absorbed power and temperature increase at any point of the resistive coating as seen in Figure 4.10.

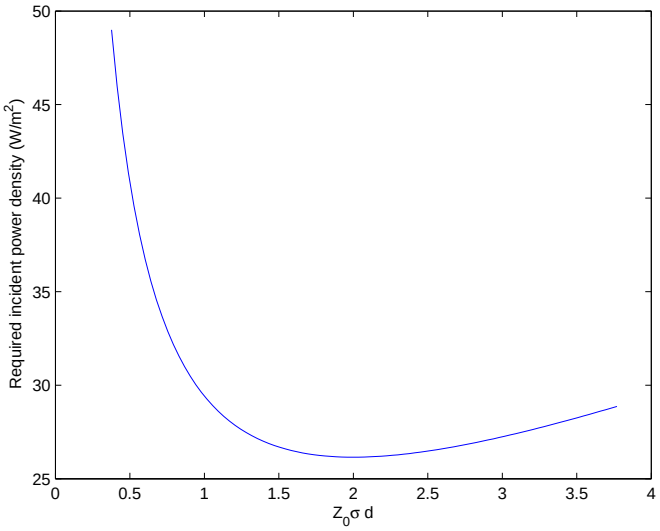

Figure 4.11: Required incident power on the screen for a 1 K temperature increase vs. $Z_0\sigma d$ product.

We have already demonstrated that only a fraction (α) o the incident power is actually absorbed into the resistive material. Therefore, a factor to take into account is the alpha parameter, dependant at the same time on thickness and conductivity. We can fix a value for desired temperature increase, such as 1 K, which offers a certain amount of contrast even in low-end IR cameras. In this case we can study how the σd product affects the necessary incident power density. This is represented in Figure 4.11 where we can clearly visualize that the minimum necessary incident power is achieved with the optimal absorption coefficient ($\alpha = 0.25$) at $Z_0\sigma d = 2$. In this particular situation the incident power density has to be of 26.15 W/m^2 to achieve a 1 K increase on the screen.

4.7.2 Temperature increase delay

Taking into account the expressions studied in the previous section, we should characterise the delay in the build up of heat on the resistive coating. In fact, it is basic to note that a sudden increase in the incident power on the screen does not translate into an immediate stable temperature. There is a transitory state where temperature rises and eventually reaches the final value, the expression of which we have already calculated.

The speed at which temperature increases for a particular power density determines the use of the screen. Furthermore, the slower the temperature builds up, the less effective this characterisation method is in comparison to standard antenna pattern determination.

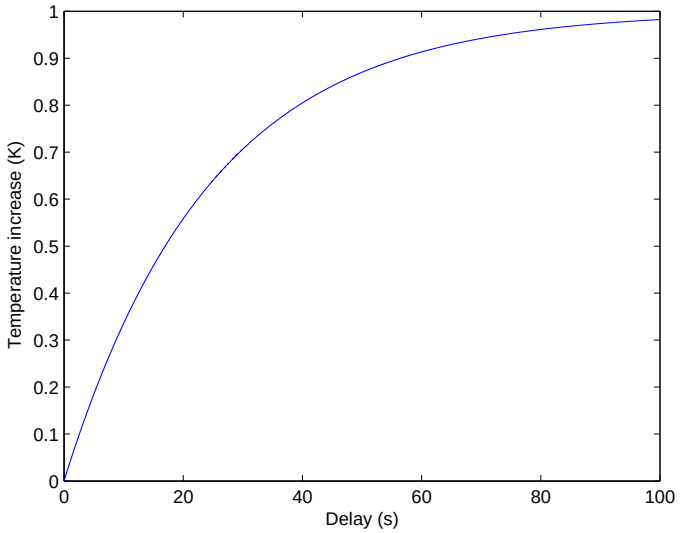

Figure 4.12: Time delay in build up of temperature for a 6.54 W/m^2 absorbed power (1 K temperature increase limit).

We can simulate this transitory state implementing the power loss expressions (previously determined). In this sense we need to evaluate the expressions for the specific heat of the material under study. The equation that describes the build-up of temperature in function of time on the screen for a particular absorbed power is

$$C\frac{\mathrm{d}T_s}{\mathrm{d}t} = \frac{P_{abs}}{A \cdot d} - \frac{P_{loss}(T_s)}{A \cdot d} = \frac{P_{abs}}{A \cdot d} - \frac{h(T_s - T_a)}{d} - \frac{\varepsilon_{ir}\sigma_b(T_s^4 - T_a^4)}{d} \tag{4.21}$$

where C is the specific heat of the material in J/(cm^3·K). This constant depends on the material, for graphite is in the 1 - 2 J/(cm^3·K) range, and for most plastics is in the 2 - 3 J/(cm^3·K) range. Therefore for our screen it is approximated as 2 J/(cm^3·K)

The result for the previous example of a 1 K temperature increase can be seen in Figure 4.12. In this particular conditions the systems response can be approximated as:

$$T(t) = T_{final}(1 - e^{-\beta t}) = T_{final}(1 - e^{-0.04t}) \tag{4.22}$$

For this particular case the response would have a time constant of $\tau = \frac{1}{\beta} = 25s$ (to achieve 63 % of its final value). These results prove the validity of the concept for a real time visualisation, as the delay in the build up is in the order of seconds, and the higher the final temperature the earlier detectable values are achieved, even with low-end IR cameras.

Chapter 5

Coating conductivity variation

On the previous chapter we have dealt with the expressions and parameters that describe how power is absorbed on the conductive coating of the visualisation screen. We have demonstrated that for a particular medium impedance Z_0 the amount of absorbed power is only dependant on two variables: the conductivity of the coating material (σ) and its thickness (d). We have also shown that there is an optimal region of values, of the σd product that provides the maximum coefficient of absorption ($\alpha = 0.25$).

The studied expressions allow us to characterize a particular coating and determine how it performs in the visualisation of antenna patterns through thermographic imaging, the method under study in this project. It is predictable however, that for a particular studied material its combined conductivity and thickness might offer values far from those required for an optimal behavior of the resistive screen. We should therefore study methods or systems to modify the value of one or both of the parameters in order to adjust the absorption coefficient into suitable (if not optimal) values.

We can take as an example the graphite coated paper used by Norgard. Its conductivity was of 8 S/m and its thickness was of 80μm. Taking into the account the expressions of the previous chapter, the sheet resistance of this coating would be 1562,5Ω. Evaluating the expression of absorption coefficient in these values we obtain $\alpha = 0.10$ which is far under the optimum value, and only offers a 10% absorption in comparison to the achievable 25%. As previously stated, in the following pages we study what strategy we can use in order to modify the σd product to obtain desired values of absorption coefficient.

5.1 Tunable variables

There are two variables that affect the absorption coefficient, conductivity and thickness of the coating. Thickness depends on the method employed to create the coating on the screen. We can assume that it can be extremely complicated to control the depth of the coating, especially when dealing with the $10\mu m$ order, and as already mentioned in [5] it is also cumbersome to determine its value once the coating has been created. We face the possibility that we might have a valid

method of ensuring a certain value of thickness, but only one, or within a limited discrete range.

The other variable affecting absorption is conductivity. It is intrinsic to the coating material and therefore, on a first approach, we can rule it out as modifiable. However, it can be argued that while the characteristic conductivity of the material might be fixed as long as the material remains untouched, we can actually modify the sheet resistance of the resistive screen as a whole, and if we do this by maintaining thickness, we are apparently modifying the conductivity according to the previously studied equivalence

$$R_S = \frac{1}{\sigma d} \tag{5.1}$$

In the following section we discuss how this is possible and methods to implement it into our thermography system.

5.2 Coating patterns

On the test set-up we have proposed, the conductive screen's surface holds currents which are induced by incident microwaves. These currents build up heat on the screen due to the Joule effect. The stronger the incident field the higher the generated currents on a certain area and the higher the temperature generated. The intensity of generated currents and incident field are linked by the screen's sheet resistance, as expressed in Chapter 4 through the transmission line analogy.

Resistance can be described as a measure of the difficulty currents find in flowing through a certain object. The easier currents flow (higher current for a certain potential difference) the lower the resistance. In our model we deal with sheet resistance which applies to thin resistive films and provides a means to characterize its resistance as a function of its geometry,

$$R = R_S \frac{L}{W} \tag{5.2}$$

where W is the width of the film and L its length, as depicted in Figure 5.1. As can be clearly seen, when dealing with a squared geometry R_S becomes equivalent to R. We therefore assume that our resistive screen is of squared proportions.

Taking into account the previous concepts we can conclude that to modify the coating's conductivity we must alter the ease with which currents flow through it. With this objective we propose to modify the approach to the coating's structure. While we have been assuming that the resistive screen is formed by a rigid body coated with a solid film of conductive paint, we study the possibility to have the coating form a conductive pattern, with void non-conductive spaces which alter the current flow and therefore increase the sheet resistance as seen in Figure 5.2.

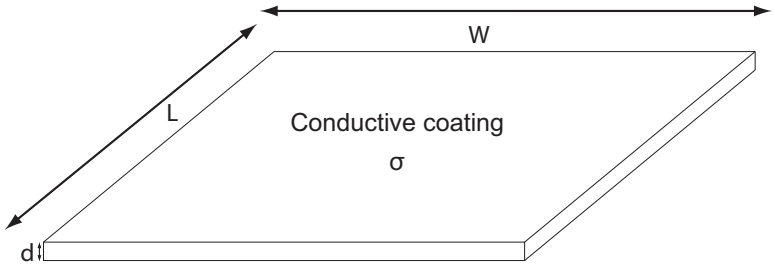

Figure 5.1: Resistance of a thin film is a function of its sheet resistance and its proportions. Sheet resistance can be approximated as $\frac{1}{\sigma d}$.

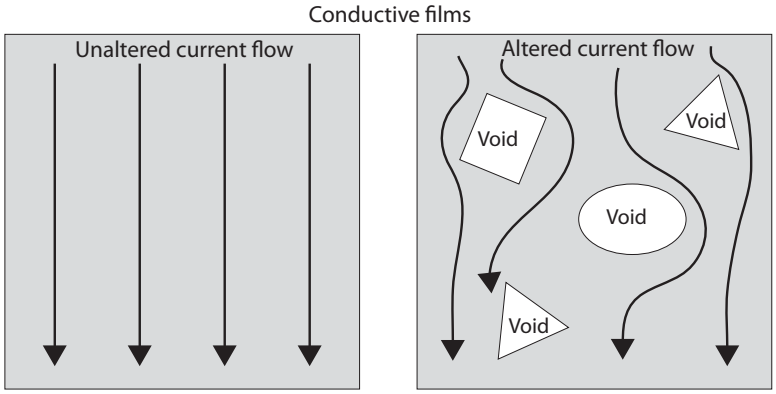

Figure 5.2: In order to modify the conducting properties, the ease with which currents flow through the coating must be modified. This can be achieved through insulation voids which deviate the paths of currents.

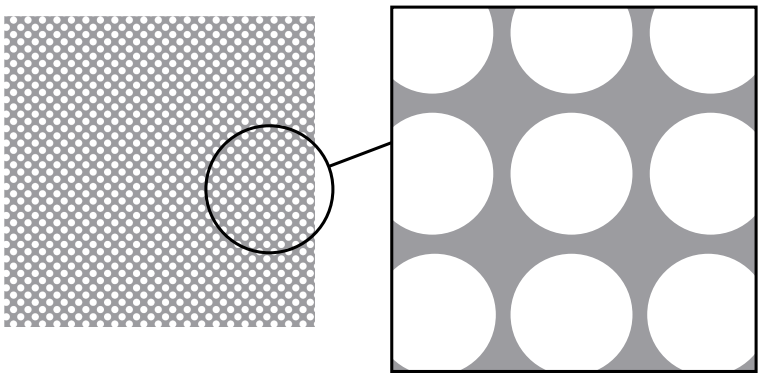

Figure 5.3: We propose a pattern of void spaces on the coating that modifies the current flow increasing the sheet resistance.

We therefore propose a method to alter conductivity through a pattern of void spaces on the conductive surface instead of a solid coating. This spaces are created with a grid of periodic circles as seen in Figure 5.3.

With the objective of characterizing how resistance is affected by the presence of the void spaces, we simulate our coating on a finite element analysis software, precisely on the *COMSOL Multiphysics* "Conductive Media Module". Initially, we instruct the software to create a conductive squared section of material. This section is assigned a thickness of 80 μm, such as the screen used by Norgard. However, as we have proved, in the mentioned experience the conductivity (8 S/m) was lower than the optimal for its particular thickness, therefore we set this value to 100 S/m (assuming that the voids method only provides the means to lower conductivity). Consequently we hope to find how the size of these isolation voids increases the resistance allowing for an optimal value of sheet resistance to be achieved.

A squared proportions section is created as previously stated. A constant 1 V potential difference is applied between two opposing sides, while the other two are set to electric insulation. In this conditions the electric induced current follows Ohm's Law

$$R_S = R = \frac{V}{I} \tag{5.3}$$

and COMSOL provides means to determine the total current that flows through one of the conducting boundaries. Therefore, we can determine, for the simulated section, its resistance.

On a first approach we evaluate the resistance of the whole section without any voids. The resistance drawn by the described method is coherent with the sheet resistance approximation

$$R_{sim} = 125 = \frac{1}{\sigma d} = \frac{1}{100 \cdot 80 \cdot 10^{-6}} \tag{5.4}$$

Subsequently a script is generated where a circular void space is created on the center of the sheet. Iterations are run with increasing radius of the insulating space, and for each value sheet resistance is stored on a position in a vector. This way we obtain a vector of resistances together with their equivalent empty circle radius.

It is worth noting that while the proposed simulation deals only with a section of the resistive pattern, containing only one empty space, we can extend the validity of the results to the large scale, due to the periodic nature of the pattern. In this sense the resistance properties remain independent of the scale at which we study the pattern as long as we maintain the proportions (Figure 5.4).

The effect of this void circles in the middle of the sheet is to pose difficulties to current flow, forcing it into the conducting edges of the sheet. In this sense the bigger the void, the higher the developed resistance. We can visualize this effect in a series of snapshots of the simulation showing current density on its surface plot in Figure 5.5.

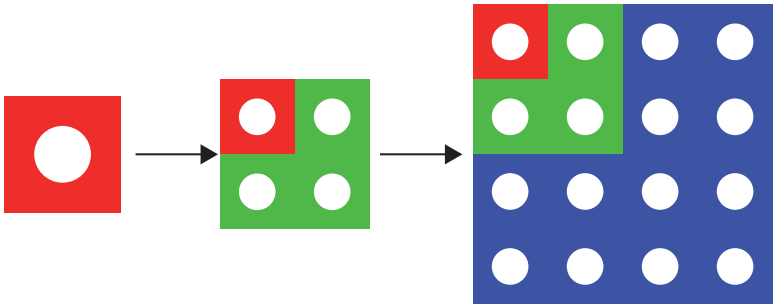

Figure 5.4: The simulation of sheet resistance of the coating can be performed on a square section comprising one only void space as the pattern is periodic.

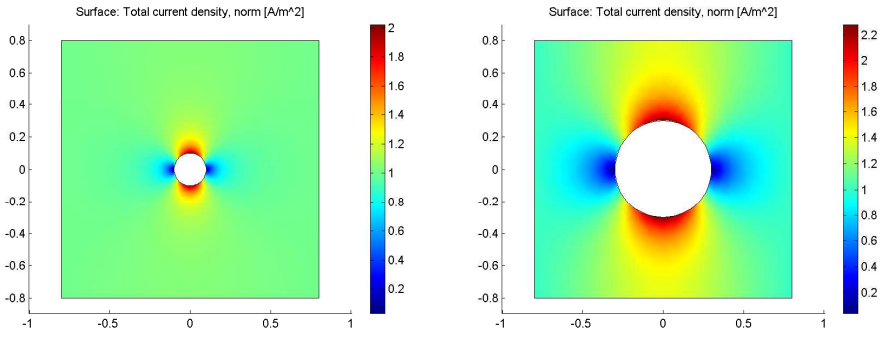

(a) Hole size: 0.1 m

(b) Hole size: 0.3 m

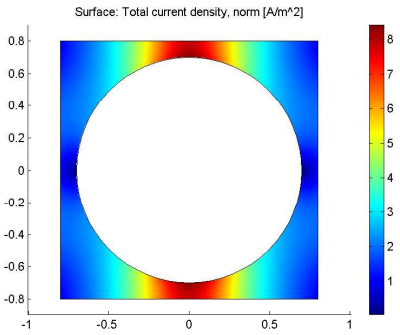

(c) Hole size: 0.7 m

Figure 5.5: Plot of the variation of surface current density on the resistive sheet as the insulating void is enlarged (current flows sideways in relation to the figure's orientation).

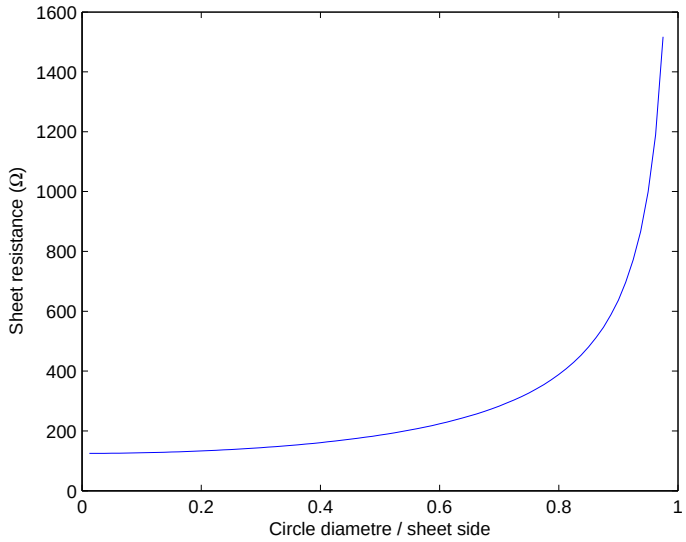

Figure 5.6: Plot of the increase of sheet resistance with the size of the insulating holes.

After running the script with 70 iterations we can create a plot that shows the dependance of developed sheet resistance versus the size of the hole. Figure 5.6 shows this dependance where resistance has been normalized to the initial void-lees value, and size of the hole is expressed as diametre/square side.

From the plot we can clearly see a slight increase for the first steps of the hole size increase, and a fast build up of resistance for bigger sizes, where diameter is approximately bigger than 0.7 times the sheet side.

The simulation shows that the resistance of the resistive coating can be effectively controlled, as long as the conductivity is determined and the thickness is kept constant. In our simulated scenario, for a 80 μm thickness and 100 S/m conductivity we can conclude that we could reach an optimal sheet resistance (regarding power absorption) with holes of a diameter 0.5 times the size of the sheet's side.

These results make us conclude that in the proposed experimental set-up, a pattern with holes on the conductive coating may be used to tune the surface's sheet resistance to provide optimal values of power absorption. The main limitation in this case would be the availability of a coating material with a conductivity higher than the one that would provide the optimal absorption.

Furthermore, if a range of discrete values of thickness could be available for one precise coating, (with a known conductivity) a value of thickness with a lower-

than-optimal resistance could be chosen. Then the pattern method could be used to elevate the sheet resistance up to the optimal value.

It is worth noting that the main requirement for this method is related to the size of the void spaces. In order not to alter the absorption of microwaves, the coating should remain solid from an electric point of view, that is, the size of the holes should remain electrically small. In this sense the proposed pattern must be regarded as one having holes much smaller than the working wavelength.

Chapter 6

Practical implementation

6.1 Coating material

In order to validate the results obtained theoretically in the initial chapters of this thesis, during its duration a series of practical tests were performed. Their final objective was to obtain a working prototype of the resistive screen to be tested for the infrared thermography procedure on our frequencies of interest (1 - 10 GHz).

The main and first concern was to decide which material would be used as the resistive coating at the root of our concept. We turned to the previous experiences on this field to obtain an approximation of valid materials. In general, the technique had usually relied on graphite coated papers for the detector screen. These papers were obtained through educational material distributors, as they are intended for current mapping in teaching at high school or on the first years of electrical engineering courses.

In the experiences conducted at the Technical University of Catalonia[5], the paper used was branded as *SAFIR* and obtained through an importer from the USA. Though the importer was contacted, the delivery delay due to batch shipping from the USA and their cost ruled out obtaining this material.

In most of the experiences conducted at the University of Colorado, the paper used was named *Teledeltos*. The precise parameters of this paper were 80 μ m of thickness and 8 S/m of conductivity. In Chapter 5 we proved that this values are not optimal for power absorption. Again, an extensive research proved inviable to have this paper shipped to Sweden.

At one point, paper branded as carbon-coated was purchased and shipped to Sweden. This paper however, when tested for conductivity proved to be highly insulating, due to the fact that regardless of the branding it was actually coated by plastic-like substances.

6.2 Creating a conductive coating

The use of previously coated papers also poses a series of disadvantages. One of the most relevant is that thickness and conductivity, the most determining values for our technique, are fixed by the make of the paper and not modifiable. Another problem is that the maximum size of one screen is limited to the size of the paper. To create a bigger screen would mean to join two or more sheets of paper. Due to these drawbacks, and also the difficulty in obtaining suitable conductive papers, our approach was reoriented towards crafting our own coating.

The first intentions were to obtain resistive paint which to coat onto our detector screen. Extensive research was undertaken. Once again however, the main hurdle found was the commercial unavailability of the appropriate materials. Though some distributors were marketing paints with determined resistance for applications such as EM shielding or circuit painting, most of them were of extremely high cost, taking into account the fact that they had to be shipped in most cases from the USA. Moreover, in general the range of available conductivities was not suitable for our needs.

Finally it was decided that we would create our own resistive paint with widely available materials. The main concern was what the paint would be based on. However, examining existing experiences with this technique and literature regarding resistive coatings such as [14], the common element proved to be graphite. Graphite is widely used for resistance purposes. In fact it is the general resistive element in variable resistances, and graphite tracks are sometimes used to create resistances that variate with length. It therefore became the focus of our efforts.

Eventually, graphite powder was purchased from an arts and crafts retail store in Barcelona. Graphite powder is commonly used in drawing for shading. In the same store acrylic paint was purchase. The objective was to test if graphite powder retained a certain conductivity when mixed with acrylic paint and used to coat a surface. Both materials appear in Figure 6.1.

6.3 Coating tests

By using arts tools, the graphite powder and the acrylic paint were mixed on an initial test. The resulting paste is extremely thick and difficult to work with. The main problem is that it is extremely complex to ensure that a thin regular coating is obtained. A 5x5 cm sample was created by coating a piece of thick poster paper. It can be seen in Figure 6.2.

In order to test the sheet resistance of a squared sample several options exist. One usual approach is to cover to opposite edges of the sample with two thin patches of aluminium foil. A current is forced from one to another, and the voltage it induces in the two farthest edges (not covered by the foil) is measured.

Figure 6.1: Graphite powder and acrylic paint were combined to create a resistive paint.

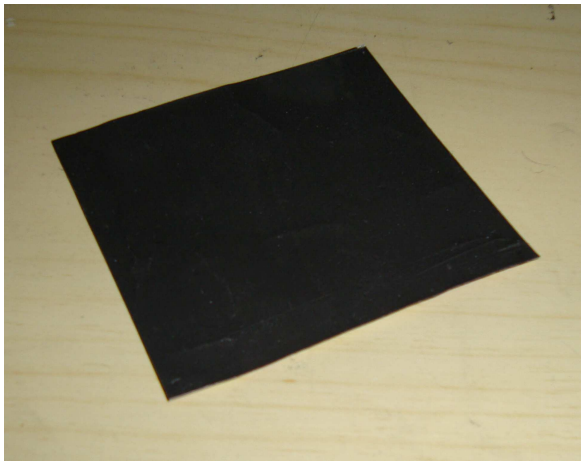

Figure 6.2: Photograph of the initial 5x5 cm sample with a resistance of approximately 1 KΩ.

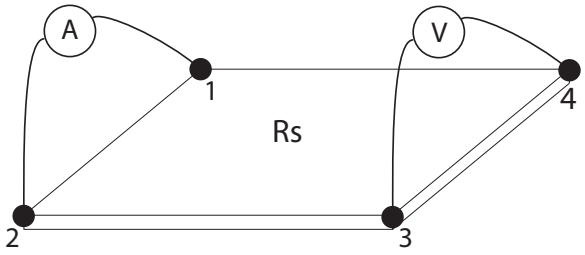

Figure 6.3: Scheme of the procedure to determine sheet resistance through the Van der Pauw method.

Then, the sheet resistance can be obtained through Ohm's law.

$$R_S = R = \frac{V}{I} \ (square\ geometry) \tag{6.1}$$

Another method that can be employed is the *Van der Pauw Method* [18]. This technique is based on numbering the edges of the sample we want to determine the sheet resistance of. Two measures are taken of the current and voltage in two correlative edges on the opposite side as depicted in Figure 6.3.
Consequently the sheet resistance is obtained solving the expressions

$$R_A = \frac{V_{43}}{I_{12}} \tag{6.2}$$

$$R_B = \frac{V_{14}}{I_{23}} \tag{6.3}$$

$$e^{-\pi \frac{R_A}{R_S}} + e^{-\pi \frac{R_B}{R_S}} = 1 \tag{6.4}$$

The sheet resistance of the first crafted sample was measured with the Van der Pauw method and a value of 1 KΩ was obtained. Even though this value is far from the optimal, it is better than the one obtained with Teledeltos paper in Norgard's experiments. Moreover, this sample proved the feasibility of our approach: graphite powder mixed with acrylic paint produced a coating with achievable resistance values in the order of those required by the technique under study.

In order to visualize relevant portions of the radiation pattern farther than the Fraunhofer distance, a bigger screen was required. With this objective a 30x30 cm piece of poster board was taken as the screen's base. One drawback we found was that in order to coat a bigger surface it was extremely complex with standard painting tools to achieve a smooth layer. With the objective to ease the process, a relatively liquid paint was crafted, with a moderate amount of graphite. The resistance of this second screen was tested and the results were in the order of the 100 KΩ. It was concluded that the amount of graphite on the paint had a very relevant effect on the resistance.

One third 30x30 cm screen was coated. This time the acrylic paint was saturated of graphite, even though the clear difficulty in the painting process. A

Figure 6.4: Photograph of the 30x30 cm detector screen obtained by coating a piece of poster board. A resistance of 250 Ω was obtained.

relatively smooth coating was obtained, even though the surface showed a rough texture probably as a result of the high concentration of graphite. The measured sheet resistance of the third screen was 250 Ω. This value was the nearest achieved to the optimal 189 Ω, and it would have provided an almost maximum absorption of 24,51 %. Therefore, in this sample an extremely suitable screen was obtained. A photograph of this sample can be seen in Figure 6.4.

The poster board employed on the bigger sized screens, and provided by the Department, was branded as *KapaFix*, and proved to be an excellent base for the resistive paint. This screen was not tested due to lack of available microwave power sources that would have provided sufficient power density at any distance with standard gain available antennas.

Chapter 7

Conclusions and future work

7.1 Conclusions

Reviewing the results obtained along this thesis we can extract conclusions regarding the system under study. Initially we have achieved a simplified approximation on the design parameters for the detector screen, based on a transmission line equivalent. This approximation has been used to express the absorption of power as a function of the two main design parameters (thickness and conductivity) and the optimal values for this parameters have been established as seen in Chapter 4.

Furthermore we have expressed through very simple approximations based on existing works on this technique, the relation between absorbed power and temperature increase on the detector screen. While approximate values for some of the system's parameters have been used, the results provide a good estimation of the orders of magnitude with which the system deals. It is worth pointing that the results obtained using these very simple expressions are in coherence with those obtained in other works where more elaborate and complex approaches have been taken[5].

The cited results point to one of the main drawbacks of the present system: in order to achieve relevant temperature differences for a clear visualisation, relatively high power densities might be required to incide the detector screen. This means that regarding the test equipment, a high-power source or a high-gain antenna (or a combination of both) might be needed. Therefore the feasibility of the system is arguable for low-directivity antennas and low-power sources.

Regarding the characteristics for real-time visualisation, we have proved that detectable temperature increases can be observed in a reasonable amount of time, in the order of seconds, and it basically depends on the applied power. This is a demonstration that the system is feasible for continuous real-time monitoring of radiation patterns as long as certain delays are tolerated for heating and cooling down of the detector screen.

On a more technical level, we have also demonstrated through simulation, how patterns on the resistive coating might be used for the optimization of the

system. The main requirement of this method would be to achieve an initial sheet resistance lower than the optimal value.

Finally, we have made a resistive paint which would suit the requirements of the system under study, using inexpensive and available materials. This paint has been used to build prototypes of the detector screen which have offered, at least on the final models, highly suitable values of sheet resistance.

7.2 Applications

Regarding the applications of the system, the main and more obvious would be to create a set-up for fast qualitative determination of antenna patterns. As opposed to actual techniques, companies or institutions could set in their anechoic chambers detector screens and infrared cameras for initial determinations of antenna patterns, which could give a broad approximation of how a particular device behaves.

The data gathered could be of deep interest and save time and resources if it prevented a further testing by the standard method. It can be argued that with a very precise set-up where the dynamic margins of the system are well-known, and the temperature-power equivalences are precisely established, the radiation patterns obtained could achieve high fidelity levels, and they could be obtained in a fraction of the time of those obtained through traditional probe measurements: one only IR image would free the chamber for the next test, thus antennas could be characterized at an industrial pace.

One consideration to make regarding the proposed set-up is that we have during this project been refereing to the detector screen as a flat surface. In fact, this is not an optimal geometry for it as it implies that for very large screens the distance between the source and the edges of the screen is higher than at the center. The optimal geometry for the screen would be of constant radius, thus following an imaginary sphere with origin on the antenna.

Moreover, we can comment on the final objective of this thesis that was to visualize antenna patterns on real time. This opens immense possibilities as the effects of modifications on antennas could be detected immediately on the IR signature. In this sense, the changes in a radiation pattern could be observed if tests were performed on a variable geometry antenna for example.

In Chapter 3 we mentioned that a total representation of the radiation pattern would require the movement of the screen around the antenna under test. We can also take into account an optimal situation where detector screens could be manufactured with the cited curved geometry. In this case, with the necessary resources, the system could be set-up with a kind of spherical screen covering all or a major angle around the antenna, forming a kind of radome. In this case a number of cameras (taking into account the risks of undesired reflections) could be used for a full representation of the radiation pattern, without the need to move

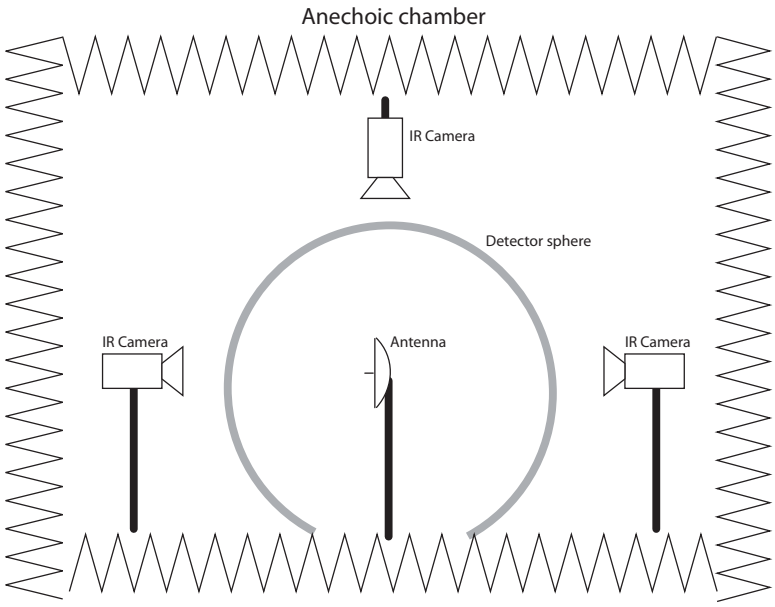

Figure 7.1: Full visualisation of an antenna pattern could be achieved with a number of cameras imaging a sphere-shaped detector screen covering the antenna under test.

either the antenna or any other element within the chamber. A mockup of this set-up can be seen in Figure 7.1.

The possibilities of this system are especially relevant when regarding phased array antennas. It could be used for instance to detect deviations on the steering of beams in 1D and 2D phased arrays, it could also be used to diagnose certain flaws on the weight or phase shifting of the single elements as unexpected pattern shapes could be their symptoms. Furthermore we must not forget the possibilities of the system on near-field testing for phased arrays, as the detector screen at a very short distance from an array would detect the radiation from each individual element thus it could be used as a fast-diagnosis tool, detecting non-radiating elements on arrays. This could be of use for fast diagnose on weather RADARs on aircraft nose cones: fast on-site tests could be performed placing the detector screen in front of the radar and taking an IR image to determine instantly if elements are not radiating.

7.3 Future work

A number of future developments appear as follow-ups of the present thesis. The most relevant would be to actually run tests with sufficiently powered antennas on the existing prototype screens. Commercial high-gain horn antennas, together

with relatively low power sources, and low-end IR cameras should be able to detect temperature differences on the point where the main beam incides. The screen could therefore be precisely calibrated, as a matter to characterize its exact temperature-power equivalence. This could lead to relatively precise radiation pattern determinations. Also, the numerically determined values for transient delay should be tested for accuracy. If the delay proved to be in a suitable order of magnitude, actual tests of varying patterns could be performed to observe them in real-time. This could be achieved with simple unidimensional phased arrays.

Eventually, the coating method should be perfected. It has been proved that a high concentrate mix of graphite powder and acrylic powder achieves excellent results regarding resistance. This mixture, however, has a very thick consistence, and becomes difficult to apply on a surface. Different methods to apply the coating should be studied.

Finally, we suggest the study of the effect of thinners on the mixture, in order to obtain a more liquid paint. If this is successful, a thin flat coating could be obtained through industrial serigraphy techniques. Also, the coating of curved surfaces could be studied in order to implement the spherical screen described in the previous section.

References

[1] "IEEE standard definitions of terms for antennas," IEEE Std 145-1983, 22 Jun 1983, URL: http://ieeexplore.ieee.org/stamp/stamp.jsp?arnumber=30651 &isnumber=1290

[2] A. Cardama; L. Jofre; J. M. Rius; J. Romeu; S. Blanch; M. Ferrando, *Antenas*, Edicions UPC, 2nd edition (2002).

[3] "IEEE standard test procedures for antennas," ANSI/IEEE Std 149-1979, 1979, URL: http://ieeexplore.ieee.org/stamp/stamp.jsp?arnumber=19510 &isnumber=768

[4] E. F. Knott; J. F. Shaeffer; M. T. Tuley, *Radar Cross Section, Second Edition*, Arthech House, Inc, 1993.

[5] J. M. González, "Caracterización de Antenas Mediante Termografías de Infrarrojos", Ph.D. Thesis, Universitat Politècnica de Catalunya, Barcelona (Spain), 2000.

[6] J. M. Gonzalez; A. Aguasca; J. Romeu, "Infrared Thermograms Applied to Near-Field Testing", IEE Electronics Letters, 1999, vol. 35, no.11, pp. 885-886.

[7] J. M. Gonzalez-Arbesu; S. Blanch; A. Aguasca; J. Romeu, "Fast far-field antenna pattern determination using infrared thermograms and phase retrieval algorith," Antennas and Propagation Society International Symposium, 2002. IEEE , vol.3, pp. 710, 2002.

[8] R. M. Sega; J. D. Norgard, "Infrared Measurements of Scattering and Electromagnetic Penetration through Apertures," Nuclear Science, IEEE Transactions on , vol.33, no.6, pp.1657-1663, Dec. 1986.

[9] J. D. Norgard, "Electromagnetic magnitude and phase measurements from infrared thermograms," Aerospace Conference, 1997. Proceedings., IEEE, vol.2, pp.145-157 vol.2, 1-8 Feb 1997.

[10] J. D. Norgard; J. Will; C. F. Stubenrauch, "Quantitative images of antenna patterns using infrared thermography and microwave holography," Int. J. Imag. Syst. Tech., vol. 11, n. 4, special issue on "Advances in quantitative image analysis", pp. 210-218, Jul.-Aug. 2000.

[11] J. D. Norgard; R. Musselman, "Direct IR diagnostics of antenna aperture distributions, University of Colorado & US Air Force Academy, USA, Quantitative InfraRed Thermography, 2004.

[12] J. D. Norgard; R. Musselman, "Direct diagnostic testing of phased array antennas using infrared imaging techniques," Electromagnetic Compatibility, 2006. EMC-Zurich 2006. 17th International Zurich Symposium on, pp.292-295, Feb. 27 2006-March 3 2006.

[13] J. D. Norgard; R. M. Sega; M. G. Harrison; N. H. Pohle, "Infrared mapping of transient electromagnetic fields radiated by high power microwave pulsed sources," Nuclear Science, IEEE Transactions on , vol.39, no.6, pp.1912-1920, Dec 1992.

[14] S. D. Kalmani; N. K. Mondal; B. Satyanarayana; P. Verma; V. M. Datar, "Development of conductive coated polyester film as RPC electrodes using screen printing," Nuclear Instruments and Methods in Physics Research Section A, Volume 602, Issue 3, p. 835-838.

[15] D. Sjöberg, "Analysis of wave propagation in stratified structures using circuit analogs, with application to electromagnetic absorbers" European Journal of Physics, Vol. 29, No. 4, pp. 721-734, 2008.

[16] S.J. Orphanidis, *Electromagnetic Waves and Antennas*, pp. 160-161 URL: http://www.ece.rutgers.edu/~orfanidi/ewa/

[17] "Table of total emissivity", Omega Engineering Inc., URL: http://www.omega.com/temperature/Z/pdf/z088-089.pdf

[18] G.Steele, "The Van der Pauw Method," URL: http://electron.mit.edu/~gsteele/vanderpauw/